The Hidden Cost of Performance: How Microcontrollers Drain Batteries in Sensor-Integrating Machine Elements

Robert Fromm
Chair of Smart Diagnostic and Online Monitoring
Faculty of Engineering
Leipzig University of Applied Sciences
Leipzig, Germany
0000-0002-2905-0648

Erich Knoll
Institute of Machine Elements
TUM School of Engineering and Design
Technical University of Munich
Munich, Germany
0000-0003-3673-0403

Cedric Wagner
Institute of Automation and Information Systems
TUM School of Engineering and Design
Technical University of Munich
Munich, Germany
0009-0005-6249-2068

Karsten Stahl
Institute of Machine Elements
TUM School of Engineering and Design
Technical University of Munich
Munich, Germany
0000-0001-7177-5207

Birgit Vogel-Heuser
Institute of Automation and Information Systems
TUM School of Engineering and Design
Technical University of Munich
Munich, Germany
0000-0003-2785-8819

Faouzi Derbel
Chair of Smart Diagnostic and Online Monitoring
Faculty of Engineering
Leipzig University of Applied Sciences
Leipzig, Germany
0000-0002-7038-8157

***Abstract*—Sensor-integrating machine elements (SiMEs) represent an effective approach for condition monitoring. These systems require highly integrated electronic circuits that combine a compact form factor, long battery life, precise signal acquisition, and reliable wireless transmission under elevated temperatures. Such conditions impose strict limits on power consumption while still demanding sufficient computing capability for data preprocessing, compression, and feature extraction. This article presents measurements of several microcontrollers commonly used in SiMEs. Processing speed, energy per operation, and quiescent current were analyzed to quantify the tradeoff between computational efficiency and battery lifetime. The results show that the energy required for basic arithmetic operations varies by up to three orders of magnitude between devices. Modern high-performance microcontrollers demonstrate excellent computational efficiency but exhibit quiescent currents exceeding 100 µA at temperatures above 90°C, making them unsuitable for long-term battery operation. The presented data provide a quantitative basis for selecting suitable microcontrollers for future SiME designs, enabling an informed balance between processing capability, energy efficiency, and thermal robustness.**

Research funded by the German Research Foundation (DFG) under project number 466653706 as part of the project "Sensor-integrating Gear" (SIZA).

***Index Terms*—Sensor-integrating machine element, condition monitoring, wireless sensor networks, microcontrollers, power consumption, temperature effects, low-power design, quiescent current**

I. Introduction

Condition-based monitoring of machine elements is essential to prevent unplanned downtime and related economic or safety risks. Continuous observation of machine condition enables maintenance only when necessary, which forms the basis of predictive maintenance. Studies show that predictive maintenance reduces unplanned downtime by up to 50%. [1]

Vibration analysis is one of the most common techniques in condition-based monitoring of rotating machinery, as many mechanical faults cause measurable changes in the vibration signature of the machine [1]. Measuring vibration close to the source increases the accuracy of fault detection. Accelerometers mounted on the machine housing capture signals that have already propagated through several mechanical interfaces and are often weakened or distorted. Embedded sensors inside the machine element record vibration directly at the point of damage origin, providing data with improved damage indication capabilities. [2], [3]

This approach has led to the development of sensor-integrating machine elements (SiMEs). These are machine elements equipped with sensors and electronic circuits similar to those found in wireless sensor nodes. SiMEs can record parameters such as load, vibration, and temperature and transmit the data often wirelessly. Wireless communication is

necessary because the sensors are often located inside rotating or otherwise inaccessible components. [1]

Implementing SiMEs involves several challenges. The embedded sensor node must have an extremely compact design, and the power supply is factor. The battery life should extend months or years to minimize maintenance effort. Alternatively, energy harvesting can be employed. [1], [4]

This article examines the electronic hardware design of the SiME wireless sensor node, focusing on the selection of a suitable microcontroller. The analysis of related research in Section II shows that SiMEs employ various microcontroller architectures. Most implementations use ARM-based devices capable of performing complex data preprocessing, compression, and feature extraction, while low-power microcontrollers such as MSP430, ATmega, or PIC16 are still common for basic processing tasks [5]–[8].

Multiple SiME types generate large amounts of data. For example, acceleration measurements combined with frequency analysis can produce about 1 MB of data per recording [5]. High sampling rates are necessary to capture all relevant harmonics within the signal bandwidth [9]. The sensor-integrating gas foil bearing developed by Kliemank et al. required a sampling rate of 2.5 MHz [10]. Wireless transmission of complete raw data is highly energy demanding, which makes local data preprocessing, compression, and feature extraction essential to reduce transmission energy. [4].

Conventional machine elements can withstand extremely high temperatures, but SiMEs are limited by the integrated electronics. Primary and secondary batteries are constrained by the minimum operating temperature specified by the manufacturer. The maximum operating temperature of the integrated circuits (ICs) defines another restriction. The upper temperature ratings of ICs are typically 85, 105, 125, and 150 °C, and only a few microcontrollers are qualified for operation at 150 °C [11]. In many machines, operating temperatures remain below 85 °C [12], [13]. Though gear wear can cause temperature variations of about 20 K [13]. Only some applications exceed 100 °C [14], [15].

Therefore, the objective of this article is to investigate the interaction between the temperature-critical environment of SiMEs, their low-power requirements, and the computing needs for predictive maintenance. The objective is to compare the computing performance and power consumption of different microcontrollers. The study includes both ultra-low-power devices and high-performance architectures to support future SiME hardware development by simplifying the selection of suitable microcontrollers for specific applications.

II. State of Research

This section examines electronic hardware designs of SiMEs presented in the state of research. The primary objective is to identify microcontrollers commonly used in these systems. The reviewed publications are arranged according to the CPU cores of the applied microcontrollers.

The ATmega328P is among the most widely used microcontrollers in electronics, largely due to the popularity of the Arduino platform. Baszenski et al. [7] employed this device in their sensor-integrating plain bearings. The ATmega328P uses an 8-bit architecture. Chilibon et al. [8] developed a system for detecting wireless acoustic emissions using a PIC16F877 microcontroller with 8-bit core, too.

MSP430 microcontrollers are designed for ultra-low power applications. Their architecture is based on a proprietary 16-bit core. We used these microcontrollers in comparable applications [5], [16], [17]. The MSP430F2 and MSP430G2 families feature a simple design combined with very low quiescent currents. Devices from the MSP430F5 family were applied by Kwan et al. [6] for maximum-power point tracking of a thermoelectric generator.

Most modern microcontrollers integrate a CPU from the ARM Cortex-M family. In the state of research, we identified devices with Cortex-M0+ [9], [18]–[20], Cortex-M3 [21], [22], Cortex-M4 [23]–[25], and Cortex-M33 [10], [26].

Although only four different CPU cores are used, the microcontrollers originate from several manufacturers and product families. The first generation of our sensor-integrating gear employs the PSoC 4500S from Infineon [18]. Paterova et al. [19] used the KL25 from NXP in an environment-monitoring sensor node powered by thermoelectric generators. The NFC-capable NHS3152 from NXP was applied in the plain bearing developed by Paeßens et al. [20]. Cornett et al. [21] implemented the ADuCM3029 from Analog Devices in their machine health monitoring node. Sridhar et al. [22] based their gear tooth wear detection system on the CC2650 from Texas Instruments. Ewert et al. [25] integrated the nRF52840 from Nordic Semiconductor in a jaw coupling. The BGM220 from Silicon Labs was used in the sensor-integrating bolt presented by Riehl et al. [26]. The largest group of devices originates from STMicroelectronics [9], [10], [23].

The ESP32 from Espressif is also a common choice for wireless sensor nodes. This microcontroller integrates a custom RISC-V CPU. Paeßens et al. [20] employed this device to provide Wi-Fi and Bluetooth Low Energy connectivity in their sensor-integrating plain bearing.

The state of research shows that various microcontrollers and CPU cores are used. However, no studies were found that compare these devices in terms of processing power consumption or processing effiency. Furthermore, the quiescent current of the microcontrollers and its increase with temperature are examined within this study. Due to the limited battery size, a low quiescent current is crucial for battery-powered SiMEs.

III. Methodology

A. Microcontroller Selection

The microcontroller selection was based on the devices identified in Section II and is summarized in Table I. Devices from different microcontroller families were chosen arbitrarily, since variations in processing power consumption and quiescent current within a family are typically small. Individual models usually differ only in analog–digital converter types, number of communication interfaces, or pin count.

TABLE I
MICROCONTROLLER SELECTION

Part number	CPU	Frequency	MPY[1]	FPU[2]
ATmega328P	8-bit	16 MHz	yes	no
ESP32-D0WD-V3	32-bit RISC	240 MHz	yes	yes
MSP430F2274	16-bit RISC	16 MHz	no	no
MSP430FR2311	16-bit RISC	16 MHz	no	no
MSP430FR5994	16-bit RISC	16 MHz	yes	no
STM32L053R8	Cortex-M0+	32 MHz	yes	no
STM32L152RE	Cortex-M3	32 MHz	yes	no
STM32L452	Cortex-M4	80 MHz	yes	yes
STM32U575	Cortex-M33	160 MHz	yes	yes

[1] hardware multiplication [2] floating-point unit

From the MSP430 series, the MSP430F2274 from the F2 family was selected. In addition, the newest generation of MSP430 devices was examined. These models use ferroelectric RAM instead of the flash memory found in all other tested microcontrollers. Devices from the FR2 and FR5 families were included to represent different CPU variants and hardware configurations. The MSP430F2274 and MSP430FR2311 are the only microcontrollers in this study that lack a hardware multiplier unit (MPY).

Because the benchmark program for evaluating processing speed must be ported to each device, the investigation of different Cortex-M cores focused exclusively on microcontrollers from STMicroelectronics. Four devices with distinct CPU cores were selected. The M4 and M33 cores include floating-point units (FPUs).

B. Processing Speed

The typical processing tasks of an SiME include data preprocessing, compression, and feature extraction [1]. Algorithms such as digital filters, Fourier transforms, and neural networks depend mainly on addition and multiplication operations. The number of CPU cycles required for a single addition and multiplication was measured. Most microcontrollers provide either a timer or a SysTick unit for counting CPU cycles. Random input values and repeated executions were used to improve measurement accuracy. Particularly for software implementations of the investigated operations, runtime depends on the number of zeros in the input numbers. Each operation was repeated 102,400 times, leading to the average values are reported in Table II.

The measurements were repeated for different data types. Integer addition and multiplication were tested with word sizes of 16, 32, and 64 bit. In addition, single-precision (32-bit) and double-precision (64-bit) floating-point operations were evaluated. Double-precision measurements were not possible on the ATmega328P and MSP430FR2311 because of limited memory capacity.

All benchmarks were combined into a single C program and compiled with the default compiler provided in each manufacturer's development environment. CPU cycle counting was performed internally, and the results were transmitted via the serial interface. The counters were calibrated by measuring CPU cycles of no-operation instructions.

The CPUs support different pipeline depths. However, since the volatile keyword was applied to all variables in the C code, the benchmark program is not optimized. Because the CPU-cycle measurement is calibrated, the results reflect the additional CPU cycles required per operation. Pipeline depth is not expected to affect the measurement, since the measurement code is linear around the evaluated operation. A residual uncertainty of only one CPU cycle remains.

C. Processing Power Consumption

The processing power consumption was measured while each device executed the benchmark algorithm, using the STLINK-V3PWR power profiler. Measurements were repeated for various supply voltages within both the profiler's range of 1.6–3.6 V and the operating range of the device under test. Due to hardware limitations of the breakout board, the ESP32 was tested only at 3.3 V. All measurements were repeated for several CPU clock frequencies. The reported values represent the average active power during steady execution of the benchmark algorithm.

D. Quiescent Currents at Higher Temperatures

Quiescent currents at elevated temperatures were not measured experimentally. Performing such measurements would require custom circuit boards, since most development boards are not specified for operation above 85 °C. In addition, IC sockets tend to fail at higher temperatures. Therefore, the analysis relies on the maximum values reported in the manufacturers' datasheets. These specifications represent guaranteed limits for all devices and production batches, whereas experimental measurements would only reflect a small number of samples, likely from a single batch.

IV. RESULTS

A. Processing Speed

Table II presents the results of the processing speed measurements. The table lists the number of CPU cycles required to execute a single operation. Using the CPU frequency of each microcontroller, the processing time can be derived directly from these values.

For 16-bit addition (ADD), most devices require about ten CPU cycles. The ATmega328P is an exception because its 8-bit core and register structure demand additional cycles for integer addition operations. The 16-bit multiplication (MPY) results clearly indicate which microcontrollers include hardware support for this operation. The ATmega328P implements hardware multiplication and therefore outperforms the 16-bit CPUs of the MSP430F2274 and MSP430FR2311. The STM microcontrollers show a significant advantage, achieving up to 32 times faster multiplication than the MSP430 devices.

On the STM32 microcontrollers, 32-bit addition executes faster than 16-bit addition. Analysis of the assembly code revealed that a 32-bit addition instruction is used, while the 16-bit addition is emulated through sign extension of

TABLE II
AVERAGE NUMBER OF CPU CYCLES PER OPERATION

Device	ADD 16-bit	MPY 16-bit	ADD 32-bit	MPY 32-bit	ADD 64-bit	MPY 64-bit	ADD float	MPY float	ADD double	MPY double
ATmega328P	28	72	42	267	163	460	134	174	—	—
ESP32	11	10	10	18	22	24	11	11	67	117
MSP430F2274	10	241	20	1403	40	1795	155	368	643	2386
MSP430FR2311	11	258	20	1536	42	1922	202	420	—	—
MSP430FR5994	8	42	17	66	35	120	170	368	559	1293
STM32L053R8	15	11	5	85	13	76	102	155	175	365
STM32L152RE	12	8	5	24	17	19	35	47	66	93
STM32L452	12	8	5	19	16	15	7	7	66	76
STM32F411	12	8	5	19	17	15	7	7	65	75
STM32U575	11	7	4	19	12	14	5	5	61	78

the operands, resulting in extra cycles. For the remaining microcontrollers, the number of CPU cycles approximately doubles when the data size is doubled. This trend continues for 64-bit addition across all tested devices.

For 32-bit multiplication, even microcontrollers with hardware support require additional CPU cycles. On MSP430 devices without a hardware multiplier, the processing time increases by roughly a factor of six when the data size is doubled.

For single-precision floating-point operations, the effect of an FPU is clearly observable in both addition and multiplication. Without hardware support, floating-point addition requires more CPU cycles than 32-bit integer addition. In contrast, multiplication is slightly faster, likely due to the logarithmic nature of floating-point representation. Multiplication corresponds to exponent addition and thus requires fewer processing steps. Floating-point addition, however, demands exponent alignment, normalization, and rounding, which increase the computational effort [27]. The STM32L152RE achieves notable performance despite lacking an FPU, requiring only 35 cycles for addition and 47 cycles for multiplication.

With double-precision floating-point operations, microcontrollers with hardware support show a clear advantage. Even in this case, up to nine times more CPU cycles are required compared to single precision. Measurements of double-precision floating-point operations on the ATmega328P and MSP430FR2311 were not possible, because the required software libraries exceeded the available program memory.

B. Processing Power Consumption

To keep the analysis concise, only selected measurement curves are shown. Fig. 1 shows the power consumption of three microcontrollers over their supply voltage range. The y-axis of these plots is normalized to the CPU frequency, since power consumption scales almost linearly with frequency [4]. The first two curves illustrate the behavior of two MSP430 microcontrollers with varying supply voltage. The power consumption of the MSP430FR2311 increases nearly linearly with voltage, corresponding to an almost constant-current load. For this device, the supply current rises by only 4% over the measured range. In contrast, the MSP430F2274 behaves more like a resistive load, with the supply current nearly doubling across the same voltage range.

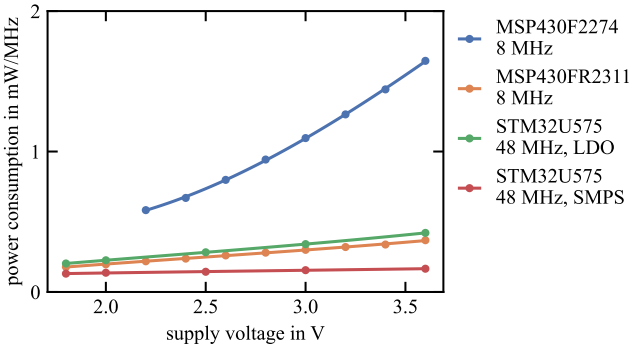

Fig. 1. Normalized processing power consumption of three microcontrollers and the STM32U575 with two internal power supply configurations

The core of the STM32U575 is powered by an internal voltage between 0.9–1.2 V, generated either by an internal low-dropout regulator (LDO regulator) or by an internal switched-mode power supply (SMPS). It is the only microcontroller in this study equipped with such an SMPS. Depending on the selected mode, the supply voltage response approximates either a constant-current load for the LDO regulator or a constant-power load for the SMPS. The power consumption curves using the LDO regulator increase linearly, similar to the behavior of the MSP430FR2322. In contrast, the curves obtained with the SMPS remain nearly constant. Besides the lower overall power consumption, the use of the SMPS also reduces the power demand significantly at a supply voltage of 1.8 V.

By combining the results of the previous measurements, the energy required for a single operation was determined. To limit the number of figures, only 32-bit integer and single-precision floating-point operations were evaluated, as these data types provide a practical balance between speed and precision. Addition and multiplication were combined into a single multiply-accumulate (MAC) operation, following the convention of digital signal processors. Eq. 1 defines the energy required for one MAC operation E_{MAC}. Here, P_{CPU} denotes the power consumption of the microcontroller, n_{ADD}

and n_{MPY} represent the number of CPU cycles required for addition and multiplication, and f_{CPU} is the CPU clock frequency.

$$E_{\mathrm{MAC}} = P_{\mathrm{CPU}} \cdot (n_{\mathrm{ADD}} + n_{\mathrm{MPY}}) / f_{\mathrm{CPU}} \tag{1}$$

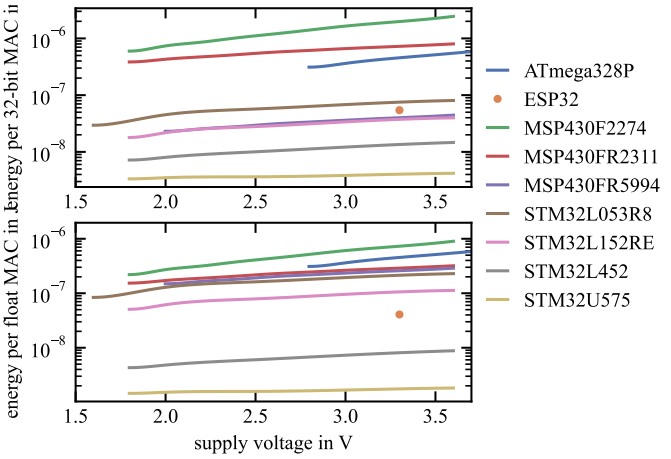

Fig. 2. Energy required per multiply-accumulate operation using 32-bit integers and single-precision floats. Voltage variation was not possible for the ESP32 due to hardware limitations of the breakout board.

In Fig. 2, this energy required per operation is shown as a function of supply voltage. In general, higher supply voltages result in increased energy demand. Despite this trend, noticeable differences remain between the investigated microcontrollers. For integer operations, the results across devices are spread out evenly. In contrast, for floating-point operations, microcontrollers equipped with an FPU show a distinct advantage. The STM32U575 exhibits the lowest energy consumption, primarily due to its internal SMPS.

However, these powerful microcontrollers operate at higher CPU frequencies and draw higher supply currents. Such current peaks can reduce power supply efficiency and accelerate battery aging. Using smaller CPUs and lower clock frequencies can mitigate these effects. For example, the STM32L452 at 4 MHz showed nearly identical energy per operation values.

All experiments were performed at room temperature, since leakage current is an additive term that has only a minor effect on total processing power consumption. This assumption is supported by device datasheets. For example, the power consumption of the MSP430FR2311 increases by only 8% at 85 °C. The datasheet of the STM32L053 shows almost no additional power consumption up to 105 °C. The STM32L452 exhibits only a small rise, about 20% at 125 °C. In contrast, the STM32U575 is highly temperature sensitive, with the maximum processing power increasing by up to a factor of ten at 125 °C. With this increase, the STM32U575 surpasses the STM32L452 in power consumption, when referencing Fig. 2.

The results presented in this investigation favor high-performance microcontrollers. However, the following subsection on quiescent currents at elevated temperatures reveals a contrasting behavior.

C. Quiescent Currents at Higher Temperatures

As explained in Subsection III-D, the results in this subsection are based on datasheet specifications rather than direct measurements. The maximum quiescent current values were taken from the lowest power mode, in which the microcontroller can still wake up via a timer or real-time clock. When available, the value corresponding to operation with an active external low-frequency oscillator (for example, a 32.768 kHz crystal) was selected. This reflects typical SiME operation, where periodic wake-up is required. For most STM microcontrollers, this mode is referred to as STOP2, and for MSP430 devices, it corresponds to LPM3.

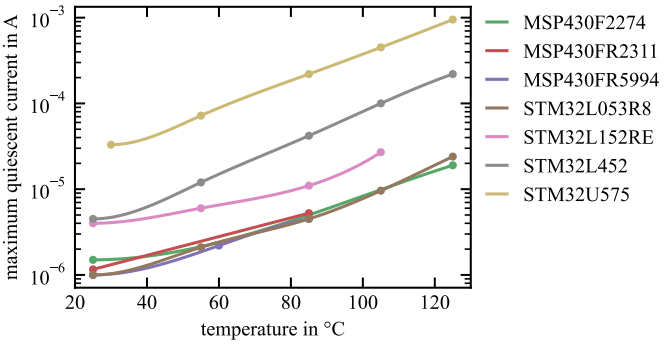

Fig. 3. Maximum quiescent current with active timer or real-time clock using an external oscillator as a function of temperature

Fig. 3 shows the maximum quiescent current from the datasheets across the typical temperature range of a SiME. No temperature-dependent values were provided for the ATmega328P or the ESP32.

Our analysis illustrates the tradeoff between processing speed and quiescent current in battery-powered applications. Even at room temperature, high-performance microcontrollers exhibit substantially higher quiescent currents. Because the plot uses a logarithmic scale, the visible linear trend represents an exponential increase in current with temperature. The slope is nearly identical for all devices, indicating that the rise is caused by semiconductor leakage characteristics [4]. Only the STM32L053 and the three MSP430 microcontrollers show low initial quiescent currents. As a result, their quiescent current increase at higher temperatures is less pronounced than that of the other devices.

Managing quiescent current is critical when a SiME is powered by a single battery intended to last several years. For example, with a 1000 mAh battery and a target lifetime of two years, the average supply current must remain below 55 µA. This average includes the quiescent current as well as the current required for data acquisition, data preprocessing, compression, and wireless communication. Consequently, devices with quiescent currents exceeding the 25 µA are unsuitable for long-term operation. In our study, only the MSP430 microcontrollers and the STM32L053 stayed below 25 µA.

V. Conclusion

Condition-based monitoring enables predictive maintenance and reduces downtime. Embedding sensors directly into machine elements has led to sensor-integrating machine elements (SiMEs), which measure vibration, temperature, or load at the area of interest. These systems face design challenges including compact geometry constraints, limited power, and high temperatures. Local data preprocessing, compression, and feature extraction reduce transmission energy. For balancing performance, efficiency, and thermal tolerance, the choice of microcontroller is crucial.

Current research shows that SiMEs use diverse microcontrollers with varying architectures and power characteristics. Most rely on ARM Cortex-M cores for their balance of speed and efficiency, while only a few employ 8-bit or 16-bit devices for ultra-low-power operation. Thermal limits also differ widely. Most SiMEs function below 100 °C. At higher temperatures, suitable ICs become scarce and leakage currents increase, reducing overall efficiency.

The measurements presented in this article determined the number of CPU cycles required for arithmetic operations such as addition and multiplication. Hardware multipliers significantly reduced the number of required cycles, particularly for 16- and 32-bit integer operations. For floating-point operations, microcontrollers with a hardware FPU achieved much shorter execution times, whereas devices without one required several times the amount of cycles. These results confirm the importance of dedicated arithmetic hardware for efficient execution of data processing.

The analysis of processing power consumption revealed distinct differences in voltage response. Some devices, such as the MSP430F2274 and ATmega328P, showed resistive behavior, where power increased with supply voltage. Most others behaved as constant-current loads, scaling almost linearly with CPU frequency but only slightly with voltage. For resistive devices, adding an external LDO regulator can reduce total power consumption, while constant-current devices benefit little from such regulators. In contrast, an internal or external SMPS effectively lowers power consumption for all devices.

The evaluation of quiescent currents showed the opposite behavior. High-performance microcontrollers exhibit high standby currents, exceeding 25 µA, which makes them unsuitable for long-term battery operation. Low-power devices such as the MSP430 series and STM32L053 maintained much lower quiescent currents, allowing multi-year operation.

Future work will address this limitation by adopting a multiprocessor architecture. A low-power microcontroller will remain active to handle timing, sensing, and wireless communication, while a high-performance device will be powered only when intensive data preprocessing, compression, and feature extraction are required. This secondary microcontroller must be fully disconnected from the supply during idle phases to eliminate leakage currents that would otherwise dominate the system's energy budget.

Data Availability Statement

The data presented in this study are openly available in FigShare at 10.6084/m9.figshare.30647915.

References

[1] E. Kirchner *et al.*, "A review on sensor-integrating machine elements," *Advanced Sensor Research*, vol. 3, no. 4, Jan. 2024.

[2] J. Peters, L. Ott, T. Gwosch, and S. Matthiesen, "Requirements for sensor integrating machine elements: A review of wear and vibration characteristics of gears," Tech. Rep., 2020.

[3] F. Strakosch, H. Nikoleizig, and F. Derbel, "Analysis and evaluation of vibration sensors for predictive maintenance of large gears with an appropriate test bench," in *2021 IEEE International Instrumentation and Measurement Technology Conference (I2MTC)*, 2021, pp. 1–6.

[4] M. C. V. Ian F. Akyildiz, *Wireless sensor networks*, I. F. Akyildiz, Ed. Wiley, Jun. 2010.

[5] F. Derbel and F. Strakosch, "Integrated sensor based smart diagnostic and online monitoring of industrial systems," in *2022 4th International Conference on Applied Automation and Industrial Diagnostics (ICAAID)*. IEEE, Mar. 2022.

[6] T. H. Kwan and X. Wu, "TEG maximum power point tracking using an adaptive duty cycle scaling algorithm," *Energy Procedia*, vol. 105, pp. 14–27, May 2017.

[7] T. Baszenski *et al.*, "Sensor integrating plain bearings: design of an energy-autonomous, temperature-based condition monitoring system," *Forschung im Ingenieurwesen*, vol. 87, no. 1, pp. 441–452, Feb. 2023.

[8] I. Chilibon, M. Mogildea, and G. Mogildea, "Wireless acoustic emission sensor device with microcontroller," *Procedia Engineering*, vol. 47, pp. 829–832, 2012.

[9] E. Knoll *et al.*, "Sensor-integrating gear wheel for in-situ measurement (SIZA)," *Forschung im Ingenieurwesen*, vol. 89, no. 1, Sep. 2025.

[10] M. L. Kliemank *et al.*, "Sensor-integrating gas foil bearings: real-time monitoring of temperature, lift-off state, and instantaneous angular speed," *Forschung im Ingenieurwesen*, vol. 89, no. 1, Aug. 2025.

[11] "AEC-Q100: failure mechanism based stress test qualification for integrated circuits in automotive applications," Tech. Rep., August 2023, revision J.

[12] A. Grzesiek *et al.*, "Long term belt conveyor gearbox temperature data analysis – statistical tests for anomaly detection," *Measurement*, vol. 165, p. 108124, Dec. 2020.

[13] T. Touret *et al.*, "On the use of temperature for online condition monitoring of geared systems – a review," *Mechanical Systems and Signal Processing*, vol. 101, pp. 197–210, Feb. 2018.

[14] Q. Lin *et al.*, "Numerical analysis of fluid and temperature field of an accessory gearbox," *Chinese Journal of Mechanical Engineering*, vol. 38, no. 1, Jul. 2025.

[15] R. Thiel *et al.*, "Gravity-based calibration for in-situ acceleration sensors," in *2025 IEEE International Instrumentation and Measurement Technology Conference (I2MTC)*, 2025, pp. 1–6.

[16] R. Fromm, O. Kanoun, and F. Derbel, "Univocal and reliable addressing patterns for wake-up receivers based on low-frequency pattern matchers," *IEEE Sensors Journal*, vol. 24, no. 8, pp. 13 431–13 438, 2024.

[17] R. Souissi *et al.*, "A self-localization algorithm for mobile targets in indoor wireless sensor networks using wake-up media access control protocol," *Sensors*, vol. 24, no. 3, 2024. [Online]. Available: https://www.mdpi.com/1424-8220/24/3/802

[18] B. Rupprecht *et al.*, "A microcontroller operating strategy for (micro) pitting and temperature increase detection in sensor-integrating gears evaluated with pre-recorded sensor data," in *2024 IEEE International Conference on Industrial Engineering and Engineering Management (IEEM)*. IEEE, Dec. 2024, pp. 1277–1284.

[19] T. Paterova *et al.*, "Environment-monitoring IoT devices powered by a TEG which converts thermal flux between air and near-surface soil into electrical energy," *Sensors*, vol. 21, no. 23, p. 8098, Dec. 2021.

[20] J. Paeßens *et al.*, "Design of a fully integrated sensor system of a plain bearing," *Forschung im Ingenieurwesen*, vol. 88, no. 1, May 2024.

[21] J. Cornett *et al.*, "Continuous machine health monitoring enabled through self-powered embedded intelligence and communication," *Journal of Physics: Conference Series*, vol. 1052, p. 012025, Jul. 2018.

[22] V. Sridhar and K. Chana, "Development of a novel sensor for gear teeth wear and damage detection," *International Journal of Prognostics and Health Management*, vol. 12, no. 3, Apr. 2021.

[23] R. Gansel *et al.*, “Identification of overloads on splined shafts by means of eddy current testing technology,” *Research and Review Journal of Nondestructive Testing*, vol. 1, no. 1, Aug. 2023.
[24] Y. Stiemcke *et al.*, “Integrated sensor system for rotary shaft seals enabling condition monitoring of dynamic sealing contact and lubricant,” *Forschung im Ingenieurwesen*, vol. 89, no. 1, Aug. 2025.
[25] A. Ewert *et al.*, “Concept of a sensor-integrating jaw coupling for measuring operating data,” *Forschung im Ingenieurwesen*, vol. 88, no. 1, Jun. 2024.
[26] D. Riehl *et al.*, “Flexible ultra-low power strain gauge readout platform for sensor-integrating bolts,” in *2025 IEEE International Instrumentation and Measurement Technology Conference (I2MTC)*. IEEE, May 2025.
[27] D. Goldberg, “What every computer scientist should know about floating-point arithmetic,” *ACM Computing Surveys*, vol. 23, no. 1, pp. 5–48, Mar. 1991.